WOOD RESEARCH doi.org/10.37763/wr.1336-4561/69.4.597610
e-ISSN 2729-8906
69(4): 2024 597 – 610 pp.

ANISOTROPIC VELOCITY MODEL AND ENERGY ATTENUATION CHARACTERISTICS OF ACOUSTIC EMISSION SIGNALS IN FINGER-JOINTED TIMBER AND SAWN TIMBER

CHUMIN CHEN[1,2,3], MING LI[4*], SAIYIN FANG[1,2,3*], BO ZHANG[5]
[1]YUNNAN KEY LABORATORY OF WOOD ADHESIVE AND GLUED PRODUCTS
[2]INTERNATIONAL JOINT RESEARCH CENTER FOR BIOMASS MATERIALS
[3]SOUTHWEST FORESTRY UNIVERSITY, YUNNAN
[4]ANHUI POLYTECHNIC UNIVERSITY, ANHUI
[5]DALIAN UNIVERSITY OF TECHNOLOGY, DALIAN
CHINA

(RECEIVED AUGUST 2024)

ABSTRACT

Although anisotropic propagation behavior of acoustic emission (AE) in the sawn timber (ST) has been revealed, that in finger-jointed timber (FJT) is still less known.Therefore, a series of velocity and energy models of AE signalswere built as it propagates along different directions on the surface and inside of specimens (ST and FJT). At first, using polar coordinate system, velocity model in 36 directions was built in FJT, which was compared to ST.Furthermore, a continuous sine wave with a frequency of 165 kHz was selected as AE source to explore the energy attenuation law in FJT and ST respectively.The results showed that there are significant differences in velocity models between FJT and ST.The wavefront in STwas regular elliptical, while that in FJT has a clear depression in perpendicular to grain direction.This feature becomes more obvious with the increase of distance when AE signal propagates inside the FJT.Inside the FJT,energy magnitude in STwas 3.00-7.37 times of that in FJT.

KEYWORDS: Propagation velocity,energy, TDOA,finger-jointed timber,sawn timber.

INTRODUCTION

The anisotropic characteristics of finger-jointed timber (FJT) make it complex to perform stress wave evaluation.Stress waves in sawn timber are independently characterized in three major directions: longitudinal (L), radial (R) and tangential (T)(Afoutou et al. 2023).In addition, adhesiveisused between the jointed timber components, which influences the propagation characteristics of the stress waves (Fruehwald-Koenig et al. 2024).Nowadays,

acoustic-based nondestructive testing (NDT) methods havebecome an effective tool for investigating the propagation characteristics of stress waves(Nasir et al. 2019), especially acoustic emission (AE) and ultrasonic methods(Wu et al. 2021b).The AE phenomenon(Holford et al. 2015), which was systematically proposed by the German Kaiser in 1953, is characterized by the rapid release of energy from a local acoustic source when a material is fractured, leading to the generation of stress waves(Iida 1981).

In AE inspection field, scholars have paid extensive attention to longitudinal propagation velocity and used it in defect localization. Qin et al. (2022)investigated the dispersion phenomenon in different sawn timbers. The phenomenon was revealed that the high-frequency signal was larger than the low-frequency signal propagation velocity when the AE signal propagated along the longitudinal direction of the four types of wood. Fang et al. (2023)explored the longitudinal and transverse wave velocities and energy attenuation models when the AE signal propagated along the longitudinal direction. The longitudinal wave was used to evaluate Young's modulus. Nevertheless, propagation characteristics of stress waves depend on the propagation direction due to the anisotropic characteristics of wood (Li et al. 2019). Currently, there is uncertainty about the relationship between stress waves and propagation direction in FJT, especially in the aspect of acoustic velocity measurements. Therefore, the study explores the propagation velocity model of AE signals on the surface and inside of the FJT, respectively.

Moreover, as an important indicator for stress wave in wood, the energy change has been widely concerned by researchers. Maoet al. (Mao et al., 2022)explored the energy attenuation characteristics of AE signals at different frequencies in wood, which showed that the energy attenuation of AE signals in softwoods is more sensitive to changes in frequency compared to hardwoods. Li et al.(2021) explored the energy decay model of stress waves as it propagates on the surface and inside the wood, and the results demonstrated that the energy decayed exponentially with the increase of the propagation distance. Xuet al.(2023)explored the changing law of AE signal energy in wood containing iron nails, revealing that the presence of iron nails reduces the ‘decay rate’ of AE signal energy. Existing studies have mainly established the attenuation law of AE signal energy with propagation distance. Actually, it is equally important to establish the AE signal energy attenuation model along different directions, confined by the natural property of wood anisotropy. This is one of the highlights of this thesis research.

Inorder to investigate the effects of anisotropy and adhesive on the propagation characteristics of stress waves in FJT, this study proposed that AE techniques were used to model the propagation velocity and energy attenuation of stress waves in the 360° direction in FJT and ST.The study building acoustic emission signal acquisition platform to collect original data based on high-speed acquisition equipment. This was divided into two parts. In the first part, the propagation velocities of longitudinal waves at different angles were calculated. The relationship between angle and velocity was derived in polar coordinates. In the second part, a fixed-frequency sinusoidal signal was emitted using a signal generator to explore the changing law of energy at different angles and to establish an energy decay model.

MATERIALS AND METHODS

Materials and equipment

In this study, Pine boards (FJT and ST) produced by a company in China were selected.FJT was named as specimen T_1 with dimensions of 500 × 500 × 15 mm (L × W × H). The length direction (L direction) was joined by finger-jointed, and the width direction (W direction) was joined by adhesive. API (adhesive polymer isocyanate) was used for joining. ST was named as specimen $T_2$with its dimensions were 260 × 260× 15 mm (L × W × H). The densities of two specimens were 535 kg/m^3 and 564 kg/m^3, respectively.

A multi-channel AE signal acquisition system was built using LabVIEW software and NI USB-6366 high-velocity acquisition device. The voltage range of the output end of the acquisition system was set to (-10 V, +10 V) during the experiment. The system was equipped with a 40 dB preamplifier. At the same time, single-ended resonant AE sensorwas selected. To ensure the full coupling between the sensor and the specimen surface, the High Vacuum greasewas used between the sensor and the surface of the specimen. According to the Nyquist sampling theorem, the original signal can be recovered without distortion only when the sampling frequency f_s is at least 2 times higher than the maximum frequency f_{max} of the original signal. Existing studies have shown that the frequency of AE signal in wood is mainly distributed in 20 kHz - 200 kHz(Xu et al. 2023).The sampling frequency f_s was set to 2 MHz so as to obtain a better resolution. In addition,in order to model the propagation velocity of stress waves, the pencil-lead break (PLB) testing was used to generate simulated AE sources.In order to explore the energy changing law at different angles, a signal generator was used to transmit a signal with a fixed frequency.

Methods for the propagation velocity models

To investigate the propagation characteristics of AE signals in FJT, the study designed the experimental scheme to build up the propagation velocity model as shown in Fig. 1.Stress waves were generated by PLB testing, the feasibility of which was demonstrated in an existing study(Wu et al. 2021).PLB testing was performed by placing a 0.5 mm diameter 2H lead core at 30° to the specimen surface and disconnecting it at a distance of 2.5 mm from the contact point. Stress waves will radiate and propagate through FJT.

A surface of the specimen T_1 (T_2) with dimensions 500×500 (260×260) was labeled as Surface A (S_A), and the surface opposite to it was labeled as Surface B (S_B).The surface center of S_A and $S_B$was used as the circle center. Concentric circles with radii of 60 mm, 120 mm, and 230 mm were selected. Simulated AE source generated at the center point in S_A.The propagation velocity of the stress wave at different angles on the surface of the specimen was calculated when the sensors (S_1-S_3) were placed on the S_A, while the propagation velocity in the inside is calculated when the sensors (S_4-S_6)were placed on the S_B. The AE signal was collected at 10° intervals in the direction of 0° - 360°.Besides, control tests were designed on ST to investigate the influence of the joining method on the propagation characteristics of the FJT clearer. Asawm timber (specimen T_2) with dimensions of 260 × 260× 15 mm (L × W × H) was taken as the experimental material. The experimental method in specimen T_2 was the same as that in T_1, except that sensors S_3 and S_6 were not placed, as

shown in Fig. 1b.

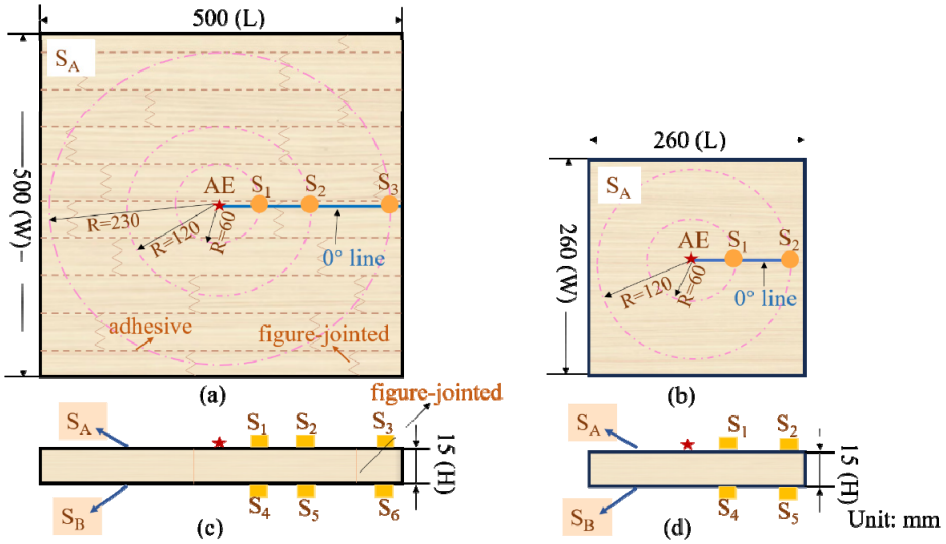

Fig.1: Experimental schematic of AE signal propagation velocity and energy at different angles. (a) and (c) are top and front views of the specimen T_1, (b) and (d) are top and front views of the specimen T_2.

With the development of AE technology, scholars used the time difference of arrival (TDOA) technique to calculate the propagation velocity of stress waves(Wang et al. 2020).The principle is to calculate the propagation velocity in a certain direction by calculating the time difference between two sensors when they first receive the signal and the distance difference between the two sensors(Fang et al. 2022).

Experimental methods for the energy changing law

This study designed an experimental scheme as shown in Fig. 2 to determine the dominant frequency of the AE signal under different splicing methods with the aim of exploring the energy change law.

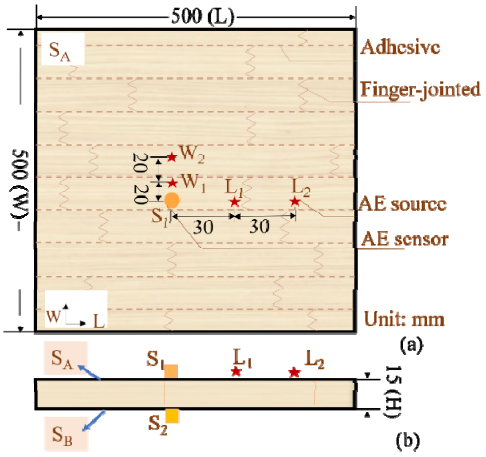

Fig. 2: Experimental schematic of the effect of adhesive on the frequency domain characteristics of AE signal.(a) Top view, (b) Front view.PLB points in L direction: L_1, L_2; PLB points in W direction: W_1, W_2.

An analogy AE source was generated through the PLB. Sensors S_1 and S_2 were placed on two surfaces, and two PLB points were selected in the L direction and W direction about sensor S_1, respectively.Different splicing methods exist between PLB points in different directions as a way to explore the frequency changing characteristics of AE signals.

Accordingly, similar to the experimental methods for propagation velocity, the study further explores the energy change law at different angles.A signal generator was used to transmit a fixed frequency sine wave signal as an analogy AE source.The placement of the sensors and the design of the experimental were the same as in Fig. 1.According to the current-thermal effect, the AE signal can be regarded as an alternating current signal and the heat generated by its passage through a unit of resistance in a fixed period of time is taken as the energy (W) of the AE signal:

$$W = \int_0^t \frac{U^2}{R} d\tau \#(1)$$

where:U is the voltage, and$R$ is the resistance.

Since the AE signals collected by the system is discrete and the time between two data is $1/f_s$ s, the energy of the AE signal can be calculated as:

$$W = \sum_{i=1}^{n} \Delta t_i \cdot u_i^2 = T \sum_{i=1}^{n} u_i^2 \#(2)$$

where:W is the energy of the AE signal; n is the data length,u_i is the amplitude of the AE signal, Δt_i=T=$1/f_s$ s, and f_s is the sampling frequency.

RESULTS AND DISCUSSION

Velocity model of AE signals

The TDOA method was used to calculate the propagation velocity of the stress wave in 36 directions. The curves of velocity (V) with angle (θ) for stress waves on the surface and inside of FJT were fitted by the least squares method in the angular intervals of [0°, 180°] and [180°, 360°], respectively, as shown in Tab. 1.

Tab. 1: Coefficients of the fitted function of velocity with angle in FJT.

	ΔS(mm)	V(m/s)	a	b	c	θ(°)	R-squared
Surface	60	V_{a1}	0.58	-103.9	5762	[0,180]	99.36%
		V_{a2}	0.56	-305	42480	[180,360]	98.46%
	170	V_{b1}	0.58	-104.3	5652	[0,180]	99.01%
		V_{b2}	0.59	-319.3	44050	[180,360]	98.19%
Inside	60	V_{c1}	0.75	-137.7	7150	[0,180]	98.06%
		V_{c2}	0.7	-379.3	52130	[180,360]	97.31%
	170	V_{d1}	0.67	-119.2	6058	[0,180]	97.62%
		V_{d2}	0.66	-356.4	48830	[180,360]	96.49%

Note: θ denotes the counterclockwise angle to the 0° line for the sensor in Fig. 1a. V_{ai}(i=1, 2), V_{bi}(i=1, 2) were measured by the sensors S_1, S_2, and S_1, S_3, respectively. V_{ci}(i=1, 2), V_{di}(i=1, 2) were measured by the sensors S_4, S_5, and S_4, S_6, respectively.

The numerical fitting model was:

$$V(\theta) = a\,\theta^2 + b\,\theta + c \#(3)$$

where: a, b, c are constants.

As seen in Tab. 1, the R-Square is greater than 96% in all cases, which demonstrates the reliability of the fitting method. Accordingly, in polar coordinates, the velocity model of the stress wave in FJT was expressed as shown in Fig. 3.Further, the wavefront of the stress wave was plotted in the right-angle coordinate system to investigate the difference between the surface and inside in the FJT, as shown in Fig. 4.The AE source was taken as the coordinate origin. the 0° and 90° directions were taken as the positive directions of x and y axes, respectively. Two times (t_1=10.5 μs, t_2=30.0 μs) were selected to represent the change law of the wavefront with time.

In Fig. 3, the curve of stress wave velocity with angle in FJT shows a symmetrical pattern with depression in the W direction and prominence in the L direction. Furthermore, in Fig. 4, comparing the changing law of the surface and inside of the wavefront with time. The intersection angles of the two wavefronts are 58.5° and 32.9° in the first quadrant when the propagation times are t1 = 10.5 μs and t2 = 30.0 μs, respectively. This suggests that the difference between surface and internal becomes more and more obvious with time.

As a matter of fact, the main reason for this difference is that the propagation velocity of the stress wave inside the FJT is more hindered. Stress waves need to be propagated by medium vibrations.In FJT, the medium includes adhesive except lignocellulose, hemicellulose, and lignin (Li et al. 2021), which characterize wood.The density of the adhesive is different from wood and creates new boundaries in the wood (Künniger et al. 2019).On the inside of the FJT, the stress waves need to traverse the adhesive and are thus impeded. Whereas on the surface of the FJT, the dimensions of the adhesive are much smaller than the dimensions of the wood fibers. Therefore, elastic waves are less disturbed by the adhesive.

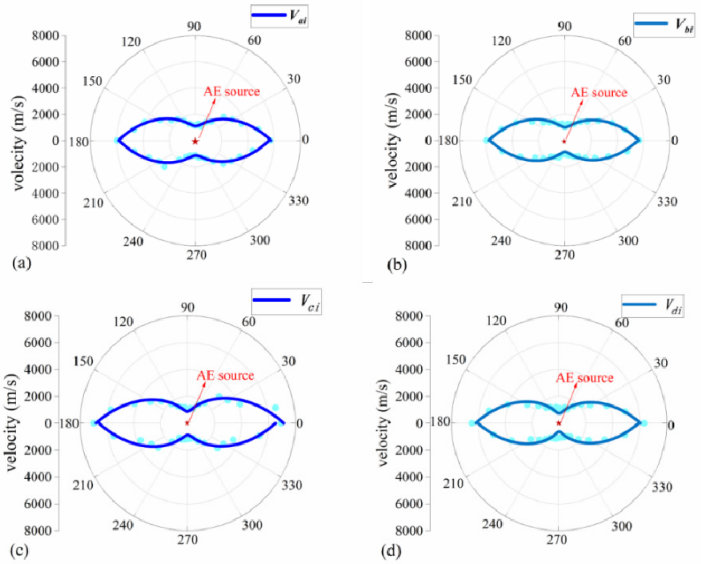

Fig. 3: Stress wave propagation velocity model on the surface and inside the FJT.(a) and (c) indicate that the AE signals propagate on the surface, and (b) and (d) indicate that the AE signals propagate in the inside.

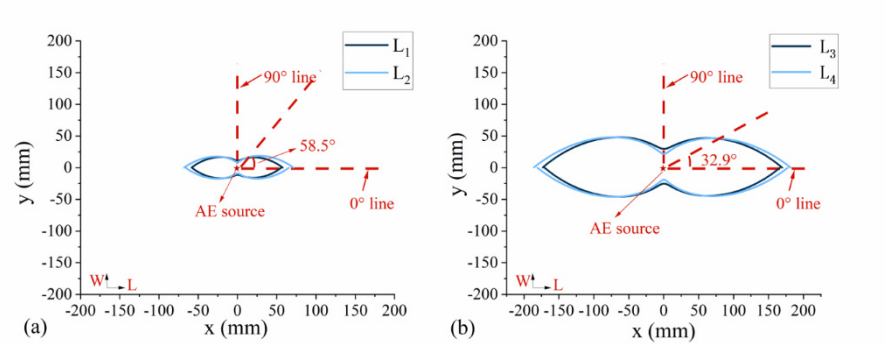

Fig. 4: Wavefront on the surface of the FJT. (a) t_1=10.5 μs, and (b) t_2=30.0 μs. L_1 and L_3 denote the wavefront when the stress wave propagates on the surface, while L_2 and L_4were inside.

For a detailed investigation of the cause of the depression features in the model, the same method was used to plot the wavefront at ST in the right-angle coordinate system for the stress wave propagation (t=1s), as shown in Fig. 5.In the field of NDT, scholars have fitted a quadratic polynomial to the change in velocity with angle over a range of 180°(Wei et al. 2020).However, according to the fitting results over 360° of the stress wave by using the AE detection technique, the wavefront of the stress wave in ST can be represented as an ellipse.The R-square is greater than 97%. The fitting function can be expressed as:

$$x^2 - 1.68xy + 8.75y^2 + 626.00x - 1470.00y - 2.07 \times 10^7 = 0\#(4)$$

$$x^2 - 1.55xy + 9.30y^2 - 253.79x + 2392.00y - 2.13 \times 10^7 = 0\#(5)$$

where: (x, y) represents the coordinates of the wavefront in the specimen; the unit of $x$and$y$ is m.

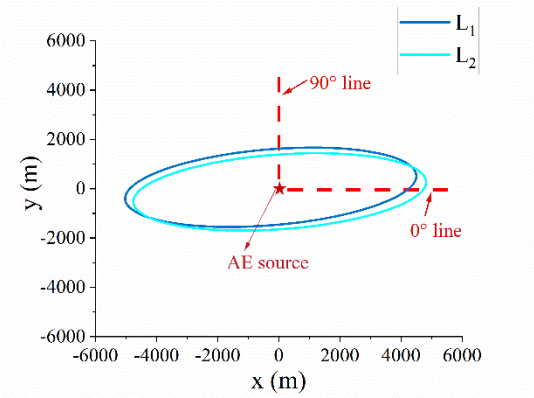

Fig. 5: Wavefront in ST. L_1 and L_2 are the surface wavefront and inside wavefront of the stress wave, respectively.

From Fig. 5, the velocity in the Parallel to the grain direction is significantly larger than that in the perpendicular tograin direction. When stress waves propagate through ST, the variability of the wavefront between the surface and the inside is inconspicuous. For details, in the L direction, $V_{L1\ max}$=4783.86 m/s, $V_{L2\ max}$=4807.59 m/s, and in the W direction, $V_{L1\ min}$=1534.88 m/s, $V_{L2\ min}$=1513.04 m/s. Wave velocity error in the same direction is less

than 0.5%.Incontrast, when the stress wave propagates through the FJT, there is a significant difference between the surface and inside wavefronts.For details, the error range is (2%, 20%) in the Ldirection and (15%, 25%) in the Wdirection.Comparing the velocity propagation models of the stress wave in the two specimens, the adhesive in the FJT significantly affects the propagation velocity of the inside stress wave, and the effect is more significant in the W direction.

Frequency domain characteristics inFJT

Same as the velocity model of the AE signal, the energy modelis also an important part in exploring the propagation characteristics of stress waves in FJT. Energy change law is explored based on analyzing the frequency characteristics of AE signal. The main frequency components of the spectrograms in the original signals collected by the AE sensors were concentrated below 20 kHz, which is due to the fact that the actual measured signals are dominated by electrical noise signals(Castro et al. 2019).On the other hand, the signals generated by PLBs were characterized by shorter duration and weaker energy, which resulted in the AE signals generated by the PLB "drowned" in the noise.Hence, a high-pass filter was used to filter the signal by setting the cutoff frequency at 20 kHz.The spectrogram of the filtered signal is shown in Fig. 6, with the main frequencies concentrated around 36 kHz (f_1) and 165 kHz (f_2).The average amplitude values of the 10 sets of data generated by the PLB were calculated and recorded in Tab.2 in order to analyzing the amplitude changes at the two main frequencies.α represents the attenuation rate at different frequency components when the AE signal passes through different splicing methods.

$$\alpha = \frac{U_2 - U_1}{U_1} \#(6)$$

where: U_1 and U_2 represent the amplitude of the main frequency components before and after the AE signal passes through the adhesive.

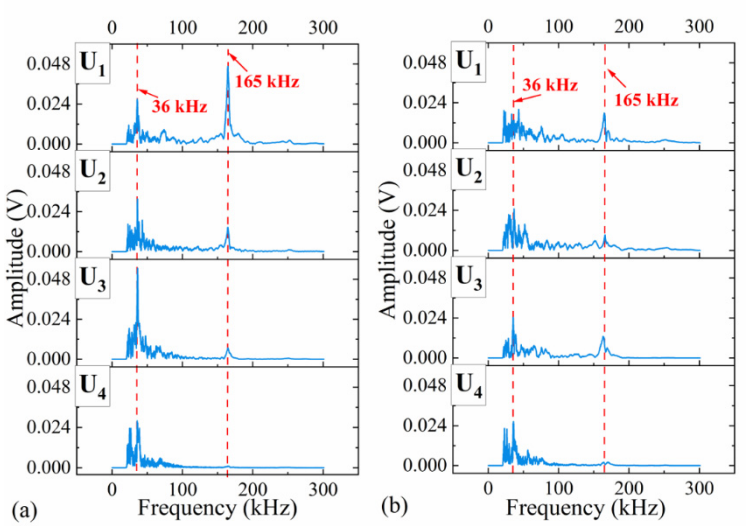

Fig. 6: Spectrograms of AE signals filtered in different directions. The signals in (a) and (b) are collected by sensors S_1 and S_2, respectively; U_1 and U_2 are generated by AE sources L_1 and L_2 in the L direction, and U_3 and U_4 are generated by AE sources W_1 and W_2 in the W direction.

Tab.2: Amplitude trend of the main frequency signal in the AE signal.

		U_1 (L)/(10^{-3})	U_2(L)/(10^{-3})	α/ (%)	U_3(W) / (10^{-3})	U_4(W) /(10^{-3})	α / (%)
Surface	36kHz	28.44	26.55	6.64	50.06	26.42	47.22
	165kHz	44.02	13.17	70.08	6.67	1.66	75.11
Inside	36kHz	21.32	20.16	5.45	27.65	15.70	43.23
	165kHz	26.59	14.57	45.19	26.28	2.33	91.20

Before the AE signal passes through the adhesive, the peak frequency is f_2 in the L direction and f_1 in the W direction, no matter whether it propagates on the surface or inside the specimen (Tab. 2).However, after the AE signals pass through the adhesive, the peak frequencies are both f_1.The adhesive creates a significant obstruction to signals with a frequency of f_2.In fact, this is caused by the phenomena of diffraction, refraction, and scattering that occur when a wave crosses the interface of two media during propagation, thus the propagation characteristics of the signal are altered(Han et al. 2020).

Energy model of AE signals

A sine wave signal with a frequency of 165 kHz was selected as the transmit frequency for the signal generator to produce the analog AE source.Compare the changing law of AE signal energy with angle when the propagation distance of stress wave is 60 mm in two specimens.The energy of AE signal with a duration of 1 μs was selected to calculate, as shown in Fig. 7.

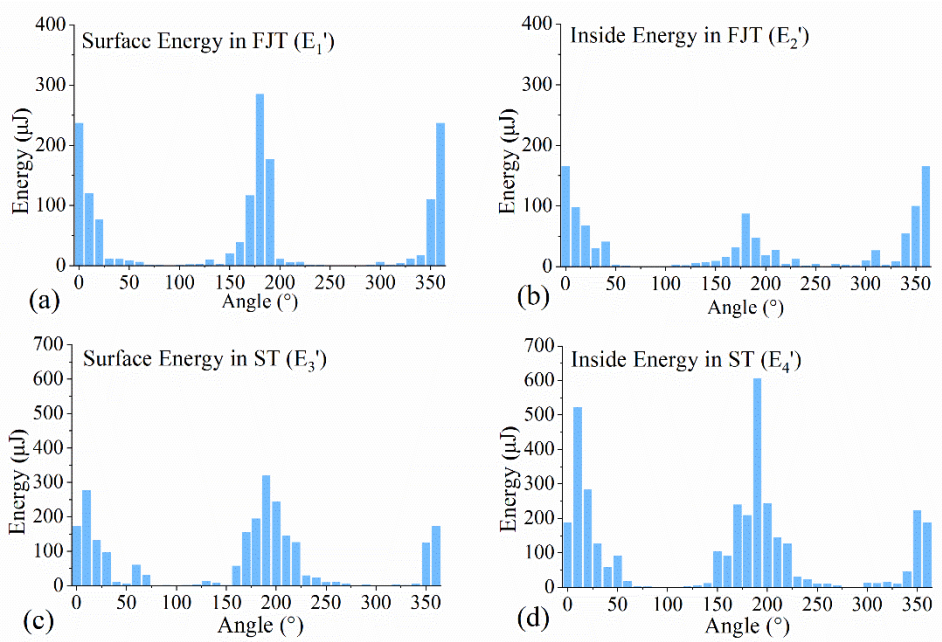

Fig. 7:The changing law of energy with angle in two specimens. (a) surface energy in FJT; (b) inside energy in FJT; (c) surface energy in ST; (d) inside energy in ST.

The energy change law in the two specimens is compared (Fig. 7). With the change of angle from L direction to W direction, the energy change law of AE signal shows an exponential decay law as a whole, and shows the phenomenon called ‘the fluctuation decay phenomenon’ with sudden increase or decrease in part of the angle.This is due to the complex

phenomena of reflection, refraction and transmission of stress waves between different media in wood(Zhao et al. 2022), which cause the wave propagation path to change and superpose at the measurement point. Therefore, the energy shows fluctuating attenuation as it changes with angle.

Additionally, in FJT, the maximum value of the AE signal energy is in the 0° or 180° direction, while that in ST is in the 10° or 190° direction. The fact is that in FJT, the 0° direction coincides with the paragrain direction. The 0° direction in ST deviates from the paragrain direction by 4.12°.This shows a clear connection between the energy of the stress wave and the wood grain. This connection is also reflected in the propagation velocity model in ST: the long axis of the ellipse has a deviation of 6.11° from the 0° line (Fig. 5).

There is a three order of magnitude difference between the maximum and minimum values of the AE signal energy (Fig. 7). Therefore, an exponential function was used to fit the energy and the results are shown in Tab.3.Specifically, the simulated AE source was used as the coordinate origin; the specimen was divided into four quadrants. In each quadrant, the paragrain direction was recorded as 0°; the perpendicular grain direction was recorded as 90°; and the angle between the measurement direction and the paragrain direction was recorded as θ. The energies at different angles were fitted. The expression of the fitting function is:

$$E' = pe^{-q\theta} \#(7)$$

where: p, q are constants; E' is the energy value of the fitted function; the unit is μJ.

Tab.3: Fitting coefficients of the energy model with stress wave propagation on the surface and inside the two specimens.

FJT	Surface (E_1')				Inside（E_2'）			
Quadrants	□	□	□	□	□	□	□	□
p	238.4	285.7	296.6	240.3	165.7	85.9	85.6	168.8
q	-0.069	-0.092	-0.085	-0.094	-0.050	-0.086	-0.056	-0.061
R^2	0.988	0.998	0.945	0.987	0.977	0.988	0.953	0.963
ST	Surface (E_3')				Inside（E_4'）			
Quadrants	□	□	□	□	□	□	□	□
p	273.6	327.4	336.1	288.3	523.4	574.4	590.7	504.3
q	-0.064	-0.053	-0.043	-0.061	-0.064	-0.061	-0.071	-0.065
R^2	0.932	0.968	0.969	0.950	0.987	0.939	0.983	0.943

According to the properties of the exponential function, the coefficient q indicates the attenuation degree of the AE signal energy.From Tab. 3, comparing the $|q|$ values in different specimens: In the FJT, the range of $|q|$ values on the surface and inside are [0.69,0.94] and [0.39, 0.86], respectively; which in the ST are [0.43,0.64] and [0.61,0.71], respectively.It is further seen that the range of the $|q|$ values in the FJTis wider, which suggests that more significant variability in the attenuation degree was caused in the different quadrants.This is because at the adhesive, reflection, refraction and diffraction phenomena occur.Different kinds of stress waves are superimposed at the AE sensor and received by it.

Moreover, the magnitude of the p-value in the exponential function symbolizes the

energy magnitude of the AE signal partially.This study compares the *p*-values of energy models for inside and surface.On the inside, the *p*-values in ST are 3.00-7.37 times higher than that in FJT, which reflects the significant inhibitory action of the adhesive on the inside energy of the AE signal.Indeed, Yanget al. (2022) regarded the wood fibers in ST as a spring one by one, and the energy of the stress wave is transmitted by the vibrations of the wood fibers,while in this study, this wood fiber, which is seen as a spring, is destroyed as the stress wave propagates in FJT.The different lumber is spliced by adhesive to build a piece of FJT. Thus, the energy will be partly absorbed when it through the adhesive, and thenthe energy is significantly reduced. As well, in the surface, the *p*-values in ST are 0.92-1.41 times higher than in FJT.Compared with the inside, the inhibiting action of the adhesive on the surface energy was not significant. That is because the surface of the specimen is contact with the air. The AE signal propagates at a free interface consisting of the surface of the specimen and air. Thus, the energy of the AE signal is less affected by the adhesive.

In recent years, scholars have characterized the energy change law of AE signals with distance, water content and other factors (Huang et al. 2022, Li et al. 2020b) into the exponential decay law.According to the results of this study, the same law is shown for the energy with wood grain.It shows obvious fluctuating attenuation phenomenon.In addition, the adhesive produces a significant suppression on the energy of the AE signal, especially the inside energy. Whether this condition could have an impact on the localization of AE sources in wood using energy or not, needs to be explored in the future.

CONCLUSIONS

The study explores the propagation characteristics of AE signals in FJT and analyzes its difference from ST.First, the propagation velocity model of the AE signal was established by generating a burst-type signal by PLB on the specimen. Second, a continuous sine wave signal with a frequency of 165 kHz was generated by a signal generator to explore the energy decay model of the AE signal.The results of the study are as follows:*(1)*In FJT, the shape of the wavefront is a symmetrical shape with depression in the W direction and prominence in the L direction. *(2)*For the propagation velocity model in FJT, the effect of the adhesive on the inside wavefront is significant, which is mainly shown that the depression of the inside wavefront in the W direction becomes more and more significant as the propagation distance changes. *(3)*As the angle increase between the propagation direction of the AE signal and the grain direction, the energy in the specimen conforms to the exponential decay law in the whole. In FJT, the adhesive leads to even more pronounced variability in the energy attenuation degree of the AE signal over different quadrants, which is reflected in the fact that the range of $|q|$ values is wider than that in ST. The adhesive produces a significant suppression of the inside energy, which is shown by the fact that the p-value in ST is 3.00-7.37 times higher than that in FJT.

In future studies, the method of localizing damage defects in FJT by combining the velocity propagation model and the energy model can be improved.

ACKNOWLEDGMENTS

This work was supported by the National Natural Science Foundation of China (32160345, 31760182), Startup fund for introducing talents and scientific research of Anhui University of Engineering (2021YQQ037), the 111 Project (2023-JNJ04) and Yunnan Fundamental Research Projects (grant NO. 202401BD070001-121).

REFERENCE

1. Afoutou, J. S., Dubois, F., Sauvat, N., Takarli, M. (2023). A novel three-dimensional model for the prediction of ultrasonic velocity in wood considering its orthotropy. Wood Science and Technology, 57(3), 605-623.
2. de Castro, B. A., Baptista, F. G., Ciampa, F. (2019). New signal processing approach for structural health monitoring in noisy environments based on impedance measurements. Measurement, 137, 155-167.
3. Fang, S., Li, M., Deng, T., Du, K. (2022). Study on the time-frequency characteristics and propagation law of acoustic emission longitudinal waves in wood grain direction. Wood Research, 67(4), 582-597.
4. Fang, S., Li, M., Li, W. E. I., Huang, C. L., Deng, T., Du, K. (2023). Experimental analysis of acoustic emission propagation velocities and energy attenuation law of P and S waves in wood using improved TDOA measurements. Wood Research, 68(1), 112-128.
5. Fruehwald-Koenig, K., Heister, L. (2024) Compression properties of glued laminated timber and tensile properties of glulam lamellas from oil palm wood. Wood Material Science and Engineering, 1-16.
6. Han, C., Yang, G., Wang, J., Guo, X. (2020). The research on propagation characteristics of acoustic emission signals in stiffened plates based on the multipath propagation model. Ultrasonics, 108.
7. Holford, K. M., Worden, K. (2015). Special issue on acoustic emission. Journal of Strain Analysis for Engineering Design.
8. Iida S. (1981). Waveform analysis of acoustic-emission. Japanese journal of applied physics. L560-L562.
9. Künniger, T., Clerc, G., Josset, S., Niemz, P., Pichelin, F., van de Kuilen, J.-W. G. (2019). Influence of humidity and frequency on the energy dissipation in wood adhesives. International Journal of Adhesion and Adhesives, 92, 99-104.
10. Li, X., Ju, S., Luo, T., Li, M. (2020a). Effect of moisture content on propagation characteristics of acoustic emission signal of *Pinus massoniana* Lamb. European Journal of Wood and Wood Products, 78(1), 185-191.
11. Li, M., Wang, M., Ding, R., Deng, T., Fang, S., Lai, F., Luo, R. (2021). Study of acoustic emission propagation characteristics and energy attenuation of surface transverse wave and internal longitudinal wave of wood. Wood Science and Technology, 55(6), 1619-1637.

12. Li, X., Ju, S., Luo, T., Li, M. (2020b). Effect of moisture content on propagation characteristics of acoustic emission signal of *Pinus massoniana* Lamb. European Journal of Wood and Wood Products, 78(1), 185-191.
13. Mao, F., Fang, S., Li, M., Huang, C., Deng, T., Zhao, Y., Qin, G. (2022). Study on attenuation characteristics of acoustic emission signals with different frequencies in wood. Sensors, 22(16).
14. Nasir, V., Nourian, S., Avramidis, S., Cool, J. (2019). Stress wave evaluation by accelerometer and acoustic emission sensor for thermally modified wood classification using three types of neural networks. European Journal of Wood and Wood Products, 77(1), 45-55.
15. Qin, G., Li, M., Fang, S., Deng, T., Huang, C., Yang, Z., Zhao, Y. (2022). Study on the dispersion characteristics of wood acoustic emission signal based on wavelet decomposition. Wood Research, 67(6), 966-978.
16. Wang, X., Liu, X., He, T., Tai, J., Shan, Y. (2020). A novel joint localization method for acoustic emission source based on time difference of arrival and beamforming. Applied Sciences, 10(22).
17. Wei, X., Sun L., Zhou, H., Yang, Y., Wang, Y. and Gao, Y. (2020). Propagation velocity model of stress waves in larch wood (*Larix gmelinii*) three-dimensional space with different moisture contents. Bioresources, 15(3), 6680-6695
18. Wu, Y., Perrin, M., Pastor, M.-L., Casari, P., Gong, X. (2021b). On the determination of acoustic emission wave propagation velocity in composite sandwich structures. Composite Structures, 259.
19. Huang, C., Li, M., Deng, T., Yang, Z., Fang, S., Xiao, S. (2022). The information entropy and fractal characteristics of acoustic emissions during wood damage and fracture. Wood Science and Technology, 56(5), 1315-1330.
20. Xu, N., Li, M., Fang, S., Huang, C., Zhao, Y., Mao, F., Wang, Y. (2023). Study the effects of ferrous materials inside wood on the propagation characteristics of acoustic emission signals. Wood Material Science and Engineering, 18(5), 1650-1662.
21. Yang Z, Huang C, Wang M, et al. (2022) Acoustic emission damage model of *Zelkova schneideriana* transverse grain compression three-point bending. Journal of Northwest Forestry University. 37(4) 238-242,256
22. Zhao, Y., Li, M., Fang, S., Zhang, S., Huang, C., Deng, T., Zhu, D. (2022). Influence of boundary conditions on acoustic emission propagation characteristics of *Zelkova schneideriana*. Journal of Wood Science, 68(1).

CHUMIN CHEN
[1]YUNNAN KEY LABORATORY OF WOOD ADHESIVE AND GLUED PRODUCTS
[2]INTERNATIONAL JOINT RESEARCH CENTER FOR BIOMASS MATERIALS
[3]SOUTHWEST FORESTRY UNIVERSITY
SCHOOL OF MACHINERY AND TRANSPORTATION
KUNMING, YUNNAN

MING LI*
[1]ANHUI POLYTECHNIC UNIVERSITY
SCHOOL OF ELECTRICAL ENGINEERING
[2]KEY LABORATORY OF ADVANCED PERCEPTION AND INTELLIGENT
CONTROLOF HIGH-END EQUIPMENT OF MINISTRY OF EDUCATION
WUHU, ANHUI
*Corresponding author: swfu_lm@swfu.edu.cn

SAIYIN FANG*
[1]YUNNAN KEY LABORATORY OF WOOD ADHESIVE AND GLUED PRODUCTS
[2]INTERNATIONAL JOINT RESEARCH CENTER FOR BIOMASS MATERIALS
[3]SOUTHWEST FORESTRY UNIVERSITY
SCHOOL OF MACHINERY AND TRANSPORTATION
KUNMING, YUNNAN
*Corresponding author: fsy029@126.com

BO ZHANG
DALIAN UNIVERSITY OF TECHNOLOGY
DALIAN, LIAONING PROVINCE
CHINA